BIOCOMPATIBLE MAGNETIC IRON OXIDE NANOPARTICLES DOPED DEXTRAN THIN FILMS PRODUCED BY SPIN COATING DEPOSITION SOLUTION

S.L. ICONARU[a], E. ANDRONESCU[b], C.S. CIOBANU[a], A.M. PRODAN[b,c,d], P. LE COUSTUMER[e], D. PREDOI[a*]

[a] National Institute for Physics of Materials, P.O. Box MG 07, Bucharest, Magurele, Romania,
[b] University Politehnica of Bucharest, Faculty of Applied Chemistry and Materials Science, Department of Science and Engineering of Oxide Materials and Nanomaterials, 1-7 Polizu Street, P.O. Box 12-134, 011061 Bucharest, Romania
[c] Carol Davila University of Medicine and Pharmacy, 8 Eroii Sanitari, sector 5, Bucharest, Romania
[d] Emergency Hospital Floreasca, Bucharest 5, Calea Floresca nr 8, sector 1, Bucarest, Romania
[e] Universite Bordeaux , EA 4592 Géoressources & Environnement, EGID, 1 allée F. Daguin 18, 33607 Pessac Cedex France

Magnetic iron oxide nanoparticles (MION) doped dextran thin films for biomedical applications have been deposited onto the glass substrate by spin coating method. To understand the influence of the MION doping dextran on physico-chemical properties was conducted. The particle concentration in the samples defined as the oxide/dextran mass ratio, R was 1 and 5. MION -dextran thin films were charcacterized by various techniques such as X-ray Photoelectron Spectroscopy (XPS), Glow Discharge Optical Emission Spectroscopy (GDOES), Scanning Electron Microscope (SEM) and Energy Dispersive X-ray Attachment (EDAX). These techniques have allowed the structural elucidation of polysaccharides thin films. The second derivative FT-IR spectra showed clearly that the polysaccharides bands. The biocompatibility of the maghemite-dextran thin films was demonstrated using MTT test, with the aid of hFOB 1.19 osteoblats cells. To evaluate cell proliferation rate quantitative by the hFOB 1.19 cells on HAp samples were cultured to 4 days. Cellular morphology was investigated using FESEM to obtain qualitative information of osteoblast cells on MION-dextran thin films. The data stronlgy suggest the potential use of iron oxide-dextran nanocomposite as a poetinal marker for or biomedical applications.

1. Introduction

Magnetic iron oxide nanoparticles (MION) are the subject of many current researches in particular because of their possible application in several areas such as biomedical applications and diagnostics [1-3]. In the last three decade, the applications of small MION (maghemite, γ-Fe$_2$O$_3$ or magnetite, Fe$_3$O$_4$) in vitro diagnostics increased. The synthesis by coprecipitation method offers some advantages: simple and rapid preparation, easy control of particle size and composition, various possibilities to modify the particle surface state allowing making homogenous and stable dispersions in liquid or solid media [4]. Nanosized γ-Fe$_2$O$_3$ transforms into α- Fe$_2$O$_3$ (hematite) at

---

rather law temperatures ($\sim 350^0$C) [5-6] but is very dependent on the history of the material [7-9]. Because of their interesting properties for biomedical applications, MION is receiving growing attention by several researchers. Moreover, it is built up by non-toxic elements, which justifies the investigation of the maghemite as thin films. Previously, the growth of MION thin films with ALD has been reported [10-11]. Methods like spin-coating, dip coating, chemical solution deposition and spray pyrolysis seem to be simpler and economic. These techniques have been widely used to prepare iron oxide thin films using various solutions [12–15]. The stabilization of the ferrofluid is achieved by optimizing the electrostatic repulsions of similarly changed surfaces. With the aim to form stable non toxic aqueous dispersion of magnetic iron oxide nanoparticles (MION), coating of the magnetic nanoparticles with biocompatible polymers has drawn recent interest.

In this paper, we describe the MION doped dextran thin films for biomedical applications deposited onto the glass substrate by spin coating method. The physico-chemical and biological properties of polymer nanocomposites thin films containing MION in a dextran matrix were investigated. Adsorption of dextran on the surface of MION was investigated by Scanning Electron Microscope (SEM) coupled with an Energy Dispersive X-ray detector (EDX), Glow Discharge Optical Emission Spectroscopy, X-ray Photoelectron Spectroscopy (XPS) and Fourier Transform Infrared (FTIR) Spectroscopy. The biocompatibility of the MION-dextran thin films was demonstrated using MTT test, with the aid of hFOB 1.19 osteoblats cells. Cellular morphology was investigated using FESEM to obtain qualitative information of osteoblast cells on maghemite-dextran thin films.

2. Experimental

2.1 Sample preparation

Ferrous chloride tetrahydrate ($FeCl_2 \cdot 4H_2O$), ferric chloride hexahidrate ($FeCl_3 \cdot 6H_2O$), natrium hydroxide (NaOH) and dextran $H(C_6H_{10}O_5)_xOH$, ferric nitrate ($FeNO_3$), nitric acid (HNO_3) where purchased from Merck, HCl these reagents were used directly asbreceived. De-ionized water was used in the synthesis of nanoparticles, and in the rinsing of clusters.

MION were prepared by co-precipitation [16-19]. Ferrous chloride tetrahydrate ($FeCl_2 \cdot 4H_2O$) in 2M HCl and ferric chloride hexahydratate ($FeCl_3 \cdot 6H_2O$) were mixed at 100 ^{0}C ($Fe^{2+}/Fe^{3+} = \frac{1}{2}$). The mixture was dropped into 200 ml of NaOH (2 mol$\cdot$L^{-1}) solution under vigorous stirring for about 30 min. The precipitate of magnetite (black precipitate immediately formed) was oxidised by repeated treatment with HNO_3 (2 mol$\cdot$L^{-1}) and $FeNO_3$ (0.3 mol$\cdot$L^{-1}) solutions [20]. The acidic precipitate was isolated by decantation on a magnet, separated by centrifugation (6000 rpm), then washed in acetone and dispersed in deionized water at pH=2.5. The final ion concentration was 0.38 mol$\cdot$L^{-1}. In a final step, the obtained product was mixed at various ratios with the different polymer solutions to obtain either iron oxide coated with dextran. For biological investigations, the pH was adjusted to 7 using aqueous amonia. The iron content of the suspensions was determined by redox-titration [21].

One millilitre of the solution is pipetted onto the substrate, and the substrate is spun at 1000 rpm for 30 s. The resulting films are annealed in a nitrogen atmosphere at 90 ^{0}C for 1 h immediately after coating and then heated at 100 ^{0}C for 1 h in vacuum to remove excess solvent and to further density the film.

2.2 Sample characterization

Transmission electron microscopy (TEM) images for these samples were recorded using a FEI Tecnai 12 equipped with a low dose digital camera from Gatan. The specimen for TEM imaging was prepared by ultramicrotomy to get thin section about 60 nm of thickness. The powder is embedded in an epoxy resin (polaron 612) before microtomy. TEM modes used were Bright Field (BF) and Selected Area Diffraction (SAD).The morphology of the material was studied using an HITACHI S2600N-type scanning electron microscope (SEM), operating at 25kV in vacuum on powder samples. The elemental local analysis was performed using an energy dispersive spectroscopy (EDS) detector from EDAX. Operating conditions were an accelerating voltage between 2 up 25 kEv (depending of the ratio signal/noise) with samples tilted at 25° to get

the optimal take off angle (30°) allowing a dead time around 20-30% and a collecting time of 90-120s. The nature of the sample avoids a conductive thin film deposition previously. The top surface analysis of the samples was studied by the Glow Discharge Optical Emission Spectroscopy (GDOES) using the GD5000 from Horiba/Jobin-Yvon. The technique is dedicated for thin film analysis and helps in determining the chemical gradient composition from the surface to the bulk and –if the ablation rate can be estimated – to precise the thickness of the different layers of the nanocomposite materials [22]. X-Ray Photoelectron Spectroscopy (XPS) studies were conducted using a VG ESCA 3 MK II XPS installation ($E_{k\alpha}$ = 1486.7 eV). The vacuum analysis chamber pressure was $P \sim 3 \times 10^{-8}$ torr. The XPS recorded spectrum involved an energy window w = 20 eV with the resolution R = 50 eV with 256 recording channels. The XPS spectra were processed using Spectral Data Processor v 2.3 (SDP) software. The functional groups present in the prepared nanoparticles and thin films were identified by FTIR using a Spectrum BX spectrometer. To obtain the nanoparticles spectra 1% of nanopowder was mixed and ground with 99% KBr. Tablets of 10 mm diameter were prepared by pressing the powder mixture at a load of 5 tons for 2 min. The spectrum was taken in the range of 500 to 4000 cm^{-1} with 4 cm^{-1} resolution. All the second derivative IR spectra were obtained after 49 –point smoothing of the original IR spectra at room temperature.

2.3 Biocompatibility tests

The hFOB 1.19 osteoblasts cells line was purchased from ATCC (American Type Culture Collection) and maintained in DMEM, containing 3,7 g/L sodium bicarbonate, 4,5 g/L D-glucose, 4,7 g/L HEPES, 4mM Lglutamine, 0,1mM sodium pyruvate, 100 U/mL penicillin, 100 U/mL streptomycin, and 10% (v/v) fetal bovine serum. Cells were grown in 5% CO2 at 37◦C and plated at 5×104cells/cm2 in Ø 100mm culture dishes with a medium change twice a week.When 70–80% confluence was reached, cells were passaged, and hFOB 1.19 cells prior to passage 4 were used in this study. Cells cultured in dishes prior to passage 3 were detached by treatment with trypsin EDTA (0.25% and 0.03%, resp.) and loaded on sucrose thin films at a seeding density of 5×104 cells/cm2 in 24-well plates. Cells cultured in 24-well plates at the same seeding density were used as control.

The cell viability was determined by MTT colorimetric assay developed by Mosmann for in vitro cytotoxicity and cell proliferation measurements [23].It was reported that the mitochondrial enzyme succinate-dehydrogenase within viable cells is able to cleave the MTT salt into formazan, a blue colored product. The amount of formazan produced, read on scanning multiwell spectrophotometer, is proportional to the number of viable cells present [23–25]. Cells were seeded at a density of 2.5×105 cells/ml and incubated by dextran-iron oxide thin films in a 12 well plate for 6 h, 24 h and 48 h. The medium from each well was removed by aspiration, the cells were washed with 200 μl phosphate buffer saline solution (PBS)/well and then 50 μl of 1 mg/ml MTT solution was added on each well. After 2 h of incubation the MTT solution from each well was removed by aspiration. A volume of 50 μl isopropanol was added and the plate was shaken to dissolve formazan crystals. The optical density at 595 nm, for each well, was then determined using a Tecan multiplate reader (Tecan GENios, Grödic, Germany). The percent of viable cells cultured on the thin film samples was calculated by reporting to a control sample, cells cultured on uncoated culture plastic vessels, considered as having a viability of 100%.

For analysis of the Actin Cytoskeleton the hFOB 1.19 cells were incubated on dextran-iron oxide thin films for 6 h, 24 h, 48 h and the culture medium was removed. Then, they were washed twice by phosphate saline buffer, and one mL of 4% paraformaldehyde was added for 20 minutes at room temperature. After three washes with phosphate saline buffer and one with 2% bovine serum albumin in 0.1% Triton X-100, a solution of 2 μg/mL phalloidin coupled with FITC in 1.2 bovine serum albumin was added. After one hour of incubation in dark, this reagent was removed. The cells were analyzed at an Olympus IX71 microscope.

3. Results and discussions

The maghemite nanoparticles synthesised by coprecipitation method as shown in Figure 1 (A). I can be seen that the particles are well dispersed and aggregation is minimal. These monodisperse nanoparticles have an average grain size of 8.3±0.3 nm. Grain size distribution were determined by measuring the mean diameter, D, of ca. 500 particles on the micrographs (Figure 1 (E)). The high-resolution TEM image in Figure 1 (B) shows the internal crystalinity for an iron oxide nanocrystal. Regular fringes are clearly observed in the nanoparticle with a spacing of 0.24 nm, which is the (311) interplanar distance of the cubic maghemite. SAED pattern of iron oxide nanoparticles in Figure 1 (C) is indexed by a cubic γ-Fe_2O_3 (PCPDF#872334), the diffraction rings are attributed to the (220), (311), (400), (422), (511) and (440) planes, respectively. Figure 1 (D) shows typical TEM images from maghemite nanoparticles coated with dextran. TEM images indicate a very uniform size distribution of dextran coated maghemite nanoparticles.
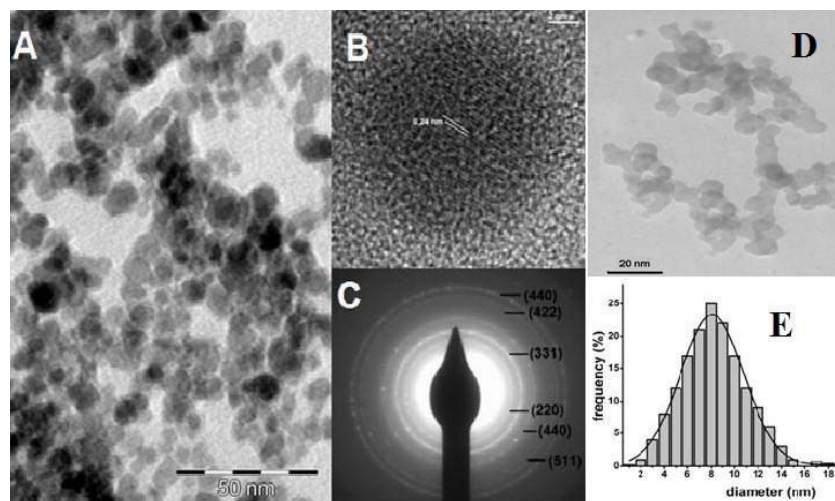
Fig.1: Synthesized maghemite nanoparticles dispersed in aqueous solution.Large area TEM image (A), High Resolution TEM image (B) and SAED pattern (C), synthesized dextran coated maghemite nanoparticles dispersed in aqueous solution (D) , size distribution of iron oxide nanoparticles (E).

Figure 2 gives the SEM and EDAX images of thin films of thin films of dextran coated MION obtained from composite targets containing 1 wt. % (A) and 5 wt. % (B) maghemite γ-Fe_2O_3. The samples consist of regular grains with some aggregation. Additionally, the grain size increased when the concentration of the maghemite NPs increased from 1wt.% to 5 wt.%**.** The SEM results reveal an obvious growing process from primary nanoparticles to the final larger products through self- assembly. The EDAX spectrum of thin films of thin films of dextran coated maghemite nanoparticles obtained from composite targets containing 1 wt. % and 5 wt. % confirms the presence of carbon (C) and oxygen (O) in all the samples. Quantitative analysis was not possible because of the glass substrate (Si peak) that affects X-EDS signal. Nevertheless, the Fe peaks observed on the spectra differ by their intensity. Regardless the concentration of dextran, the chemical composition, their distribution and morphology were not changed.
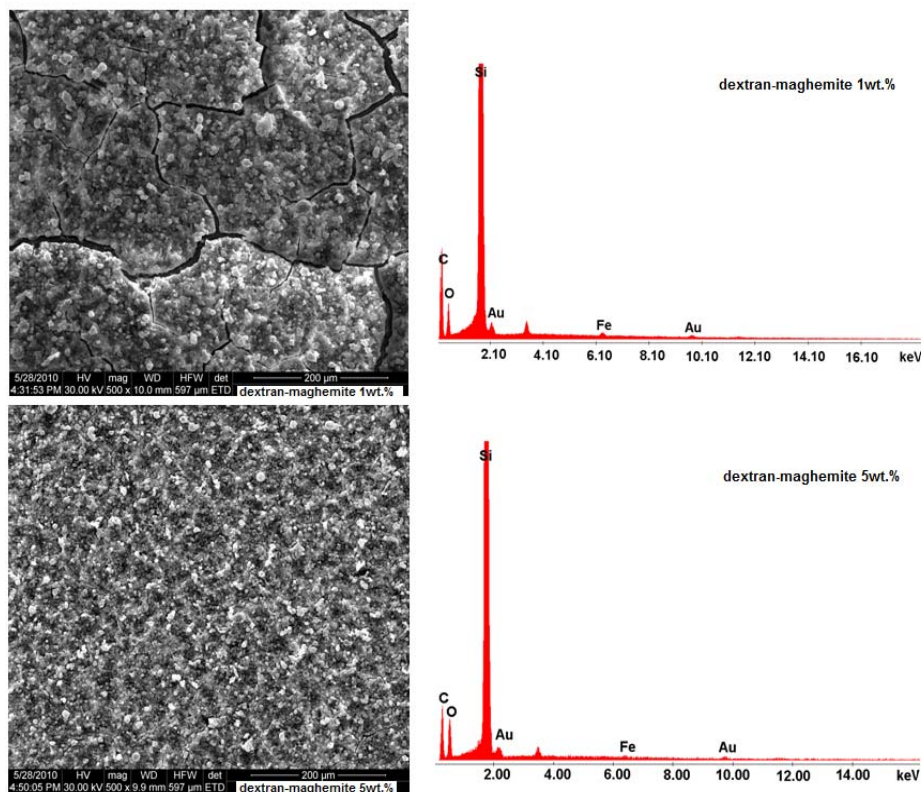
Fig. 2: SEM micrographs of thin films of dextran coated maghemite nanoparticles obtained from composite targets containing 1 wt. % and 5 wt. % maghemite.

The GDOES Spectra (figure 3) respectively performed on thin films of dextran coated maghemite nanoparticles are obtained from composite targets containing 1 wt. % and 5 wt. % maghemite γ-Fe_2O_3 deposited on a silica glass substrate. The two spectra reveal the presence of a material composed mainly of carbon, iron and oxygen. Top surface (before 10s of analytical time) corresponds to a contaminated layer (carbon oxygen mainly) frequently observed in as received material [26]. Between 10s and 180s or 140s, carbon, iron and oxygen signals increased to reach a maximum before decreasing. This zone corresponds to the nanocomposite of dextran spiked with maghemite γ-Fe_2O_3. After 180s or 140s, the signal of silicon increases corresponding to the glass substrate. Thus the signal observed between 10 s and respectively 180s for composite targets containing 1 wt. % maghemite and 140s for composite targets containing 1 wt. % maghemite, exhibit the same pattern differing only by the intensity measured. In the case of the samples with 1 wt. % maghemite the iron signal is lower than carbon which is opposite with the sample doped by 5 wt. % maghemite. The carbon signal corresponds to the dextran while iron is related to the maghemite. However, oxygen is included in both phases. Thus the sequences observed on the figure 3 tends to reveal that maghemetite is embedded by the dextran regardless the concentration. Average rate of ablation was around 2s/min. By measuring the depth of the GD crater using profilometry, the thin film thickness was estimated about 280 nm (sample doped by 5 wt. % maghemite)   and 360 nm (sample doped by 1 wt. % maghemite).
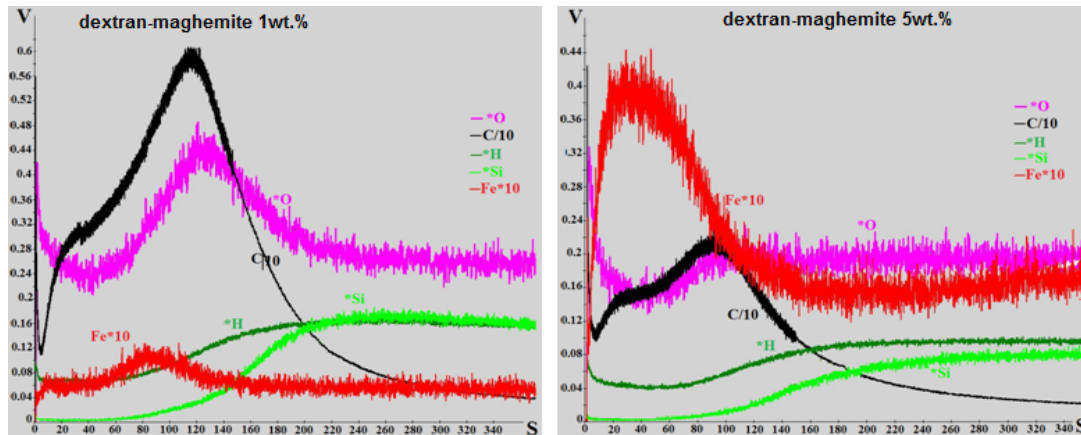
Fig. 3: Analytical results by GDOES on thin films of dextran coated maghemite nanoparticles obtained from composite targets containing 1 wt. % and 5 wt. % maghemite.

X-ray photoelectron spectroscopy (Figure 4) results are consistent with the expected composition of thin films of dextran coated maghemite, γ-Fe_2O_3.
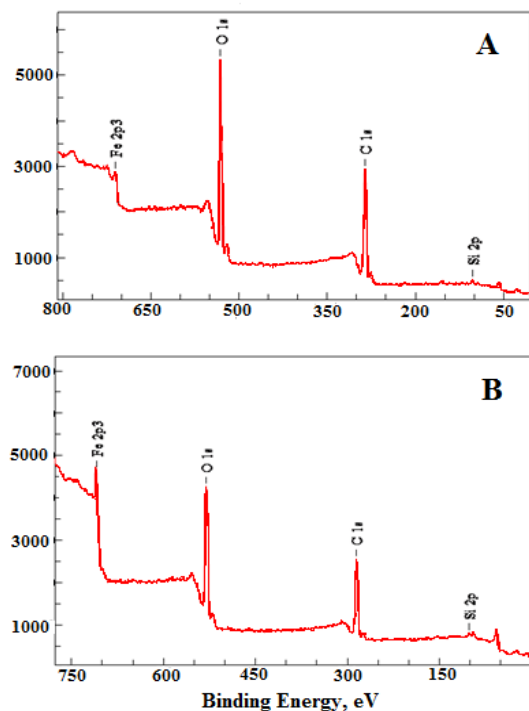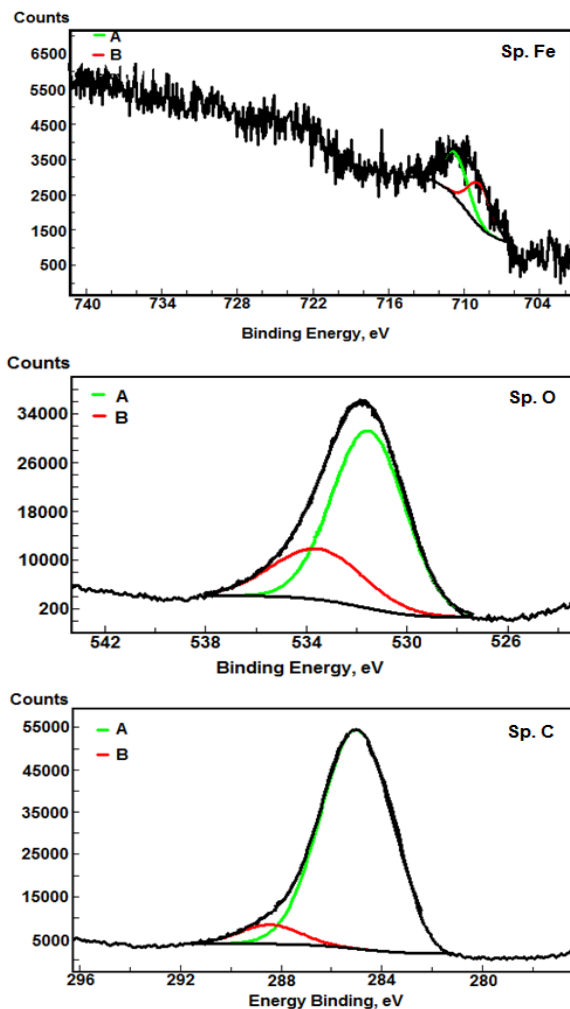

Fig. 4: XPS spectrum of thin films of dextran coated maghemite nanoparticles obtained from composite targets containing 1 wt. % (A) and 5 wt. % (B) maghemite γ-Fe_2O_3.

In the XPS general spectra of thin films dextran coated iron oxide the binding energy of Fe (2p, 710,9 eV), O (1s, 532.55 eV) and C (1s, 286.43 eV) were found. The binding energy of the O1s peak in thin films of dextran coated iron oxide is in good agreement with values for lattice O_1^- in metal oxide [27-28]. They are attributed to O_1^-, OH^- and physisorbed H_2O respectively. On the other hand the O1s photoelectrons in both thin films of dextran coated maghemite are due to dextran (C-O-C [or H]) contributions [29]. The major components of the C1s at 286,3 eV in the spectra of thin films of dextran coated maghemite γ-Fe_2O_3 are due primarily to the CHOH groups

of the dextran. The components of the Si2p in all spectra are due to the substrate contributions. The Fe 2p, O 1s and C1s XPS spectra for the thin solid films of dextran coated maghemite nanoparticles obtained from composite targets containing 5 wt. % are presented in Figure 5. Existence of doublet spin orbit component corresponding to Fe $2p_{3/2}$ and Fe $2p_{1/2}$ is presented. The Fe $2p_{3/2}$ peak was found to have binding energy bettween energy 711.2 eV and 711.6 eV and the Fe $2p_{1/2}$ peak from 725.2 to 725.8 eV. The results indicate that iron was completely in the Fe^{3+} state. The broadened shape of the O 1s spectra (Figure 5) suggests that the oxygen is present in at least two states. Figure 4 showed a typical O 1 spectrum fitted with two Gaussian components.

Fig 5: The Fe 2p O 1s and C1s XPS spectra for the thin solid films of dextran coated maghemite nanoparticles obtained from composite targets containing 1 wt. % (A) and 5 wt. % (B). The spectra were normalized to maximum intensity.

The binding energy separation is ~ 2.31 eV in good accord with literature [27]. The main peak is located at 530.58 eV. This component corresponds to O^{2-} in the iron oxide lattice [28-29]. The second component is represented by a peak located at 532.89 eV and could attributed to OH^- [30- 33] and physisorbed H_2O respectively. On the other hand the O1s photoelectrons in both thin films of dextran coated maghemite are due to dextran (C-O-C [or H]) contributions [34]. The major components of the C1s at 286,3 eV (Figure 5) in the spectra of thin films of dextran coated maghemite γ-Fe_2O_3 are due primarily to the CHOH groups of the dextran. A smaler peak at ~ 288 eV is atributable to the anometric carbone of dextran. The components of the Si 2p in all spectra are due to the substrate contributions.

FT-IR is one of the most widely used methods to identify the chemical constituents and elucidate the compounds structures. IR spectrum of all thin films shows lot of structural information of major constituents. As shown in Figure 6 in the 3600-1600 cm-1 region four bands appear: a broad band centered at 3400 cm^{-1} and 1700 cm^{-1} assigned to the OH stretching (v OH) and HOH (δ OH) vibrational bands due to the adsorbed water molecules in the sample [35], the weak signal at 2927 cm^{-1} [36-39].
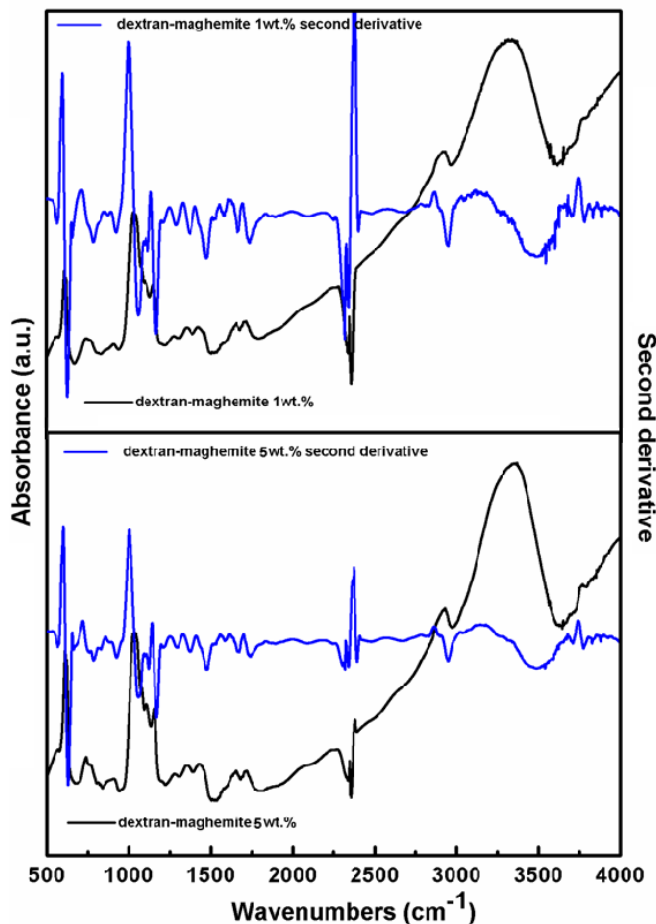

Fig. 6: FT-IR spectra and second derivative (blue) of thin film of dextran coated maghemite nanoparticles obtained from composite targets containing 1 wt. % and 5 wt. % maghemite.

The band at 1434cm^{-1} may by due to C-OH deformation vibration with contributions of O-C-O symetric stretching vibration of carboxylate group [40-41]. The stronger peacks appear in the renge of 1150-900 cm^{-1} mainly attributed to the stretching vibration of C-O-C [42]. Those characters of peaks intensities and positions at 1150, 1020, 912 and 731 in the IR spectrum display the characteristic absorptions of polysaccharides. The bands observed in the 650-550 cm^{-1} corresponds to the Fe-O vibrations modes of γ-Fe$_2$O$_3$ [43-45]. The FT-IR spectra and the second derivative spectra give more information than classical IR for polysaccharides and biomolecules contained in organism such as red seaweeds, fungi and bacteria [46-51]. Furthermore, in the second derivative spectrum the bands observed are assigned of polysaccharides.

In order to evaluate the degree of compatibility of thin film of dextran coated maghemite nanoparticles with hFOB 1.19 osteoblasts, the MTT test for short term (6, 24, and 48 hours) was performed for exploring the possible cellular toxicity at interaction with these surfaces (Figure 7).
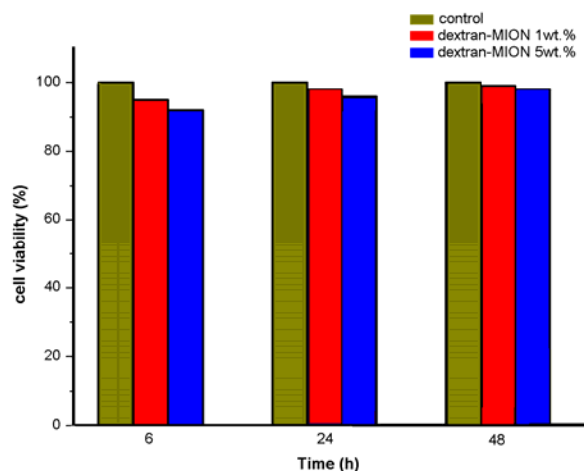
Fig.7. Viability of hFOB 1.19 osteoblasts grown on dextran thin film obtained from targets containing 1 wt. % and 5 wt. % maghemite.
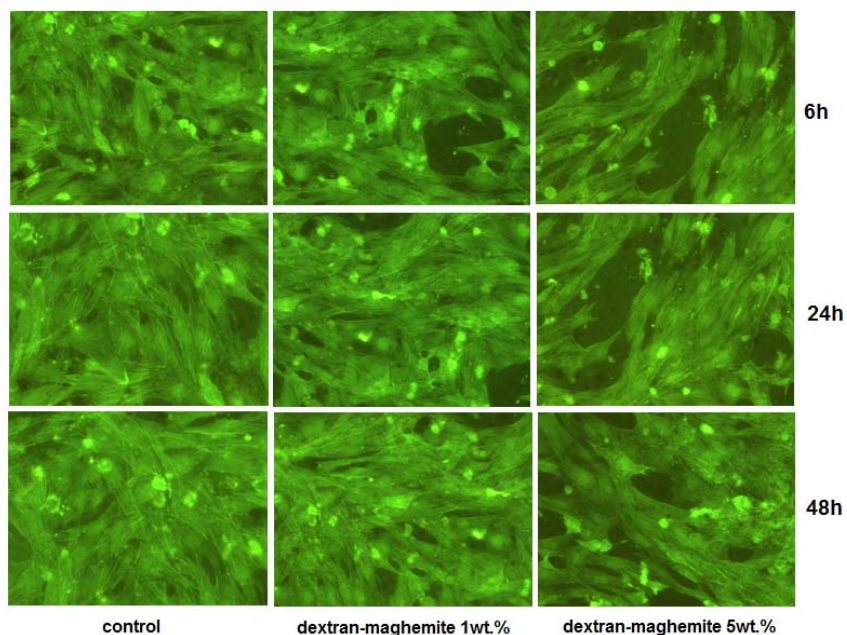

Fig. 8: Fluorescence micrograph of hFOB 1.19 osteoblasts plated on dextran thin film obtained from targets containing 1 wt. % and 5 wt. % maghemite.

Our data have shown that the viability of cells did not decrease significantly compared to control over 48 hours suggesting that osteoblasts were not damaged at the contact with the thin film of dextran coated maghemite nanoparticles.

In this study, we were interested in the expression of F-actin in hFOB 1.19 osteoblasts adhered to dextran thin film obtained from targets containing 1 wt. % and 5 wt. % maghemite. Actin is highly conserved proteins that are ubiquitously expressed in all eukaryotic cells. F-actin microfilaments are essential for the maintenance of cell shape and permeability of tight junctions [52]. Figure 8 shows that, after 48 hours of cultivation, the expression of F-actin in hFOB 1.19 osteoblasts adhered on dextran thin film obtained from targets containing 1 wt. % and 5 wt. %

maghemite was similar and less than in control cells. Also, no changes in cells morphology were noticed under phase contrast microscopy [53].

4. Conclusions

Biocompatible magnetic iron oxide nanoparticles doped dextran thin films were produced by spin coating deposition solution. This method resulted in the deposition of continuous thin films, with chemical composition and molecular structure identical to those of the starting materials used for the target preparation. By measuring the depth of the GD crater using profilometry, the thin film thickness was estimated about 280 nm (sample doped by 5 wt. % maghemite)   and 360 nm (sample doped by 1 wt. % maghemite). In XPS spectrum the Fe $2p_{3/2}$ peak was found to have binding energy bettween energy 711.2 eV and 711.6 eV and the Fe $2p_{1/2}$ peak from 725.2 to 725.8 eV. The results indicate that iron was completely in the Fe^{3+} state. The granular surface morphology represent an advantage in the adhesion and growth of living hFOB 1.19 osteoblasts cells. Our results prove that hFOB 1.19 osteoblasts adhere very well to dextran thin film obtained from targets containing 1 wt. % and 5 wt. % maghemite and exhibit a normal actin cytoskeleton, which suggest that these cells undergo normal cell cycle progression.

Acknowledgement

References

[1] S.M. Moghimi, A.C.H. Hunter, J.C. Murray, Pharm. Rev., **53**, 283 (2001).
[2] A.S.G. Curtis, C. Wilkinson, Trends Biotech., **19**, 97 (2001).
[3] J.M. Wilkinson, Med. Device. Technol 2003, **14 (5),** 29 (2003).
[4] E. Tronc, J.P. Jolivet, J. Livage, Hyperfine Interactions, **54**, 737 (1990).
[5] G. Ennas, G. Marongin, A. Musinu, A. Falgui, P. Ballirano, R. Caminito, J. Mater.Res. **14**, 1570 (1999).
[6] C. Chaneac, E. Tronc, J.P. Jolivet, Nanostruct. Mater., **6**, (1995) 715.
[7] A. Rousset, G. Boissier, J.P. Caffin and F. Chassagnes, C.R. Acad. Sci. Paris, 299, ser., **11**, 781 (1984).
[8] M. Macias, J. Morales, J.L. Tirado and C. Valera, Thermochim Acta **133**, 106 (1988).
[9] F. Mathieu, P. Roux, G. Bonel, A. Rousset, C.R. Acad. Sci. Paris, 305, ser. **11**, 249 (1987).
[10] M. de Ridder, P.C. van de Ven, R.G. van Welzenis, H.H. Brongersma, S. Helfensteyn, C. Creemers, P. Van Der Voort, M. Baltes, M. Mathieu, E.F. Vansant, J. Phys. Chem. B, **106**, 13146 (2002).
[11] B.S. Lim, A. Rahtu, R.G. Gordon, Nat. Mater., **2**, 749 (2003).
[12] A.A. Akl, Appl. Surf. Sci., **233**, 307 (2004).
[13] W.B. Ingler Jr., S.U.M. Khan, Int. J. Hydrogen Energ., **30**, 821 (2005).
[14] R.V. Todorovska, St. Groudeva-Zotova, D.S. Todorovsky, Mater. Lett., **56**, 770 (2002). [15] L. Dghoughi, B. Elidrissi, C. Bernède, M. Addou, M. Alaoui Lamrani, M. Regragui, H. Erguig, Appl. Surf. Sci., **253**, 1823 (2006).
[16] D. Prodan, C. Chaneac, E. Tronc, J.P. Jolivet, R. Cherkaour, A. Ezzir, and J.L. Dormann, JMMM, **203**, 63 (1999).
[17] R. Massart, IEEE Trans. Magn, **17**, 1247 (1981).
[18] A. Bee, R. Massart, J. Magn. Magn. Mater., **1**, 122 (1990).
[19] D. Predoi, C. Valsangiacom, J. Optoel. Adv. Mater., **9**, 1797 (2007).
[20] D.Prodan, V.V. Grecu, M.N. Grecu, E. Tronc, J.P. Jolivet, Meas. Sci. Technol, **10 (9)**, L41 (1999).
[21] S. Mornet, F. Grasset, J. Portier, E. Duguet, Eur. Cell. Mater., **3S2,** 110 (2002).

[22] P. Le Coustumer, P. Chapon, R. Payling, H. François Saint-Cyr and M. Motelica Heino, Surf & Interface Anal., **35**, 623 (2003).

[23] T. Mosmann, J. Immunol. Methods, **65**, 55 (1983).

[24] F. Denizot, R. Lang, J. Immunol. Methods, **89**, 271 (1986).

[25] H. Wan, R. Williams, P. Doherty, D.F. Williams, J. Mater. Sci. Mater. Med., **5,** 154 (1994).

[26] D. Predoi, V. Kuncser, E. Tronc, M. Nogues, U. Russo, G. Principi and G. Filoti, J. Phys.: Condens. Matter, **15(10)**, 1797 (2003).

[27] Moses PR, Wier LM, Lennox IC, Finklea HO, Murray RW, *Anal Chem,* **50**, 576 (1978).

[28] Hendewerk M, Salmeron M, Somorjai GA, *Surf Sci* , **172,** 544 (1986).

[29] Gaggiotti G, Galdikas A, Kačiulis S, Mattogno G, Setkus A, *J Appl Phys,* **76**, 4467 (1994).

[30] Kawabe T, Shimomura S, Karasuda T, Tabata K, Suzuki E, Yamaguchi Y, Surf Sci, **448**, 101 (2000).

[31] Wandelt K, Surf Sci Rep, **2**, 1 (1982).

[32] Roosendaal SJ, Vredenberg AM, Habraken FHPM, Phys Rev Let, **84,** 3366 (2000).

[33] Desai JD, Pathan HM, Sun-Ki Min, Kwang-Deog Jung, Oh Shim Joo, Applied Surface Science, **252**, 1870 (2005).

[34] Clarc DT, In *Hand Book of X-Ray and Ultraviolet Photoelectron Spectroscopy*. Edited by Briggs D. London: Heyden, 220 (1977).

[35] D. Predoi, E. Andronescu, M. Radu, M.C. Munteanu, A. Dinischiotu, Digest J. Nanom. Biostr., **5**, 779 (2010).

[36] M. C. Bautista, O. Bomati-Miguel, M. del Puerto Morales, C. J. Serna, S. Veintemillas Verdauguer, J. Magnetism and Magnet. Mater., **20**, 293 (2005).

[37] H. R. Wang, K. M. Chen, Colloids and Surfaces A: Physicochem. Eng. Aspects **281**, 190 (2006).

[38] E. Castellanos Gil, A. I. Colarte, A. El Ghzaoui, D. Durand, J.L. Delarbre, B. Bataille, Eur. J. Pharm. Biopharm., **68**, 319 (2008).

[39] M. J. Powers, R. E, Rodriguez, L. G. Griffith, Biotechnol. Bioeng., **53**, 415 (1996).

[40] M. Mathlouthi, J.L. Koenig, Adv. Carbohydr. Chem. Biochem., **44**, 7(1986).

[41] R.M. Silverstein, G. Clayton Bassier, T.C. Morrill, Spectrometric Identification of Organic Compounds: Wiley: New York, 1991.

[42] K. Lammers, G. Arbuckle-keil, J. Dighton, Soil Biol. Biochem., **41**, 340 (2009).

[43] J. L. Martin de Vidales, A. Lopez-Delgado, E. Vila, F. A. Lopez, J. Alloys. Compd., **287,** 276 (1999).

[44] D. Predoi, Dig. J. Nanomater. Biostruct., **2**, 169 (2007).

[45] J. Hradil, A. Pisarov, M. Babič, D. Horák, China Part., **5,** 162 (2007).

[46] P.J. Caceres, C.A. Faundez, B. Matsuhiro, J. A. Vasquez, J. Appl. Phycol., **8**, 523 (1997).

[47] A.J. Michell, Carbohydr. Res., **173**, 185 (1990).

[48] B. Matsuhiro, Hydrobiologia,   **326/327**, 481 (1996).

[49] B. Matsuhiro, P.Rivas, J. Appl. Phycol., **5**, 45 (1993).

[50] G. Sandt, G.D. Sockalingum, D. Aubert, H. Lepan, C. Lepouse, M. Joussaud, A. Leon, J. M. Pinon, M. Manfait, D. Toubas, J. Clin. Microbiol., **41**, 954 (2003).

[51] A. Oust, T. Moretro, K. Naterstad, G. Sockalingum, I. Adt, M. Manfait, A. Kohler, Appl. Environ. Microbiol., **72**, 228 (2006).

[52] N. Tsukada, C.A. Ackerley, M.J. Philips, Hepatology, **21**, 1106 (1995).

[53] Y.-J. Wang, R.B. Gregory, G.J. Barritt, J. Biol. Chem., **275**, 22229 (2000).